Click Here for Full Article

Ice cloud properties in ice-over-water cloud systems using Tropical Rainfall Measuring Mission (TRMM) visible and infrared scanner and TRMM Microwave Imager data

Patrick Minnis,[1] Jianping Huang,[2] Bing Lin,[1] Yuhong Yi,[3] Robert F. Arduini,[3] Tai-Fang Fan,[3] J. Kirk Ayers,[3] and Gerald G. Mace[4]

[1] A multilayered cloud retrieval system (MCRS) is updated and used to estimate ice water path in maritime ice-over-water clouds using Visible and Infrared Scanner (VIRS) and Tropical Rainfall Measuring Mission (TRMM) Microwave Imager (TMI) measurements acquired over the Tropics between January and August 1998. Lookup tables of top-of-atmosphere 0.65-μm reflectance are developed for ice-over-water cloud systems using radiative transfer calculations for various combinations of ice-over-water cloud layers. The liquid and ice water paths, LWP and IWP, respectively, are determined with the MCRS using these lookup tables with a combination of microwave (MW), visible (VIS), and infrared (IR) data. LWP, determined directly from the TMI MW data, is used to define the lower-level cloud properties to select the proper lookup table. The properties of the upper-level ice clouds, such as optical depth and effective size, are then derived using the Visible–Infrared Solar-infrared Split-Window technique (VISST), which matches the VIRS IR, 3.9 μm, and VIS data to the multilayer cloud lookup table reflectances and a set of emittance parameterizations. Initial comparisons with surface-based radar retrievals suggest that this enhanced MCRS can significantly improve the accuracy and decrease the IWP in overlapped clouds by 42 and 13% compared to using the single-layer VISST and an earlier simplified MW–VIS–IR (MVI) differencing method, respectively, for ice-over-water cloud systems. The tropical distribution of ice-over-water clouds is the same as derived earlier from combined TMI and VIRS data, but the new values of IWP and optical depth are slightly larger than the older MVI values and exceed those of single-layered clouds by 7 and 11%, respectively. The mean IWP from the MCRS is 8–14% greater than that retrieved from radar retrievals of overlapped clouds over two surface sites, and the standard deviations of the differences are similar to those for single-layered clouds. Examples of a method for applying the MCRS over land without MW data yield similar differences with the surface retrievals. By combining the MCRS with other techniques that focus primarily on optically thin cirrus over low water clouds, it will be possible to more fully assess the IWP in all conditions over ocean except for precipitating systems.

1. Introduction

[2] Satellite retrievals of ice cloud properties, essential for characterizing the global atmospheric hydrological and radiation budgets, are often complicated by the occurrence of multilayered overlapped (OL) clouds. Most current satellite cloud retrievals are based on the assumption that all clouds are comprised of a homogeneous single layer within the field of view of the satellite measurements, despite the frequent occurrence of OL cloud systems. Cloud overlap can introduce large errors in the retrieval of many cloud properties such as ice water path (IWP), cloud height, optical depth, thermodynamic phase, and effective particle size [e.g., *Huang et al.*, 2005]. For multilayered systems with ice clouds overlying water clouds, the influence of liquid water clouds on satellite-observed radiances observed

---

[1]NASA Langley Research Center, Hampton, Virginia, USA.
[2]College of Atmospheric Sciences, Lanzhou University, Lanzhou, China.
[3]Science Systems and Applications, Inc., Hampton, Virginia, USA.
[4]Department of Meteorology, University of Utah, Salt Lake City, Utah, USA.

is one of the greatest impediments to accurately determining cloud ice amount. The optical depth derived from the reflected visible (VIS) radiance represents the combined effects of all cloud layers. When the reflected radiance is interpreted using a single-layer (SL) ice cloud model, the ice cloud optical depth can be significantly overestimated because the underlying water cloud generally increases the reflectance. It is clear that the underlying clouds must be properly characterized for a more accurate retrieval of cloud properties in OL systems.

[3] To retrieve the properties of OL cloud systems, it is first necessary to identify which pixels in satellite imagery contain multilayered clouds. Several techniques for discriminating SL from multilayered clouds have been developed and applied to data taken over broad areas of the globe. Over water surfaces, the combined use of microwave (MW), VIS, and infrared (IR) data can be used to detect liquid water underneath higher clouds as long as the layers are separated by effective radiating temperatures of 8 K or more. *Lin and Rossow* [1996] and *Lin et al.* [1998a, 1998b] applied this MW–VIS–IR (MVI) method to poorly matched data sets from different satellite platforms, whereas *Ho et al.* [2003] applied it to well-matched Visible and Infrared Scanner (VIRS) and Tropical Rainfall Measuring Mission (TRMM) Microwave Imager (TMI) data on the TRMM satellite. *Pavolonis and Heidinger* [2004] developed an 11- to 12-μm brightness temperature difference (BTD) method combined with VIS imager data to detect thin cirrus clouds over water clouds and analyzed a large global data set that only excludes bright surfaces such as snow and deserts [*Heidinger and Pavolonis*, 2005]. *Chang and Li* [2005a] combined a CO_2-slicing IR method and VIS–IR data (COVIR) to detect a similar variety of OL thin cirrus above liquid water clouds over the same range of surface types and analyzed global data over 4 months spanning a single year [*Chang and Li*, 2005b].

[4] Once a pixel containing OL clouds is identified, the cloud properties in each layer need to be estimated. *Chang and Li* [2005a] took advantage of the effective emissivity of the CO_2-slicing method to assign an initial value to the ice cloud optical depth, then the VIS–IR radiances are used together with a two-layer cloud reflectance model, an IR emissivity parameterization, and contextual information to iterate to a solution for the upper and lower cloud properties. For the OL clouds detected by the MVI approach, the liquid water path (LWP) is estimated directly from the MW data providing the anchor for estimating IWP. The simplest approach to analyze the MVI-detected clouds, designated the MVI retrieval technique, retrieves the total cloud water path (TWP) using a VIS–IR technique that assumes that the entire cloud consists of ice particles. The IWP is estimated as the difference between the TWP and MW-derived LWP [*Lin and Rossow*, 1996; *Lin et al.*, 1998a, 1998b; *Ho et al.*, 2003]. Recognizing that the radiative fields emanating from combined ice and water cloud layers are generally not equivalent to those with the same TWP, *Huang et al.* [2005] developed a more rigorous multilayer cloud retrieval system (MCRS) that explicitly treats both the low-level cloud as part of the background radiation field for the upper-layer cloud and the ice cloud contribution to the top of atmosphere (TOA) radiance to estimate the IWP values. In the initial version of the MCRS, *Huang et al.* [2005] used a

parameterization of the adding-doubling (AD) radiative transfer method by combining the low-layer cloud with the surface to produce a background radiance for the retrieval of the ice cloud properties. It significantly improved the accuracy of the retrieved IWP but is subject to greater uncertainty than more exact calculations of radiative transfer [*Arduini et al.*, 2002].

[5] To reduce that uncertainty and produce a more accurate assessment of OL tropical maritime clouds, this study first upgrades the MCRS and then applies it to VIRS and TMI data. The improved MCRS uses lookup tables of reflectance based on radiative transfer calculations of combined ice and water cloud reflectance. The background in the radiative transfer model can be either a land or ocean surface. This enhanced version is more accurate and is applicable to a broader range of boundary conditions. The cloud properties and VIRS radiances from the latest edition of the VIRS retrievals by the Clouds and the Earth's Radiant Energy System [CERES, see *Wielicki et al.*, 1998] project are matched with TMI data and then reanalyzed with the MCRS. A preliminary validation of the results is performed using data from surface observations. The information derived using the MCRS should improve our understanding of the distribution of IWP and provide a reference for evaluating the IWP generated by climate models over the tropical oceans.

2. Data

[6] The data used here consist of MW, VIS, and IR measurements taken by the TRMM satellite over open oceans equatorward of 38° latitude. TRMM is in a 350-km circular orbit with a 35° inclination angle [*Kummerow et al.*, 1998]. TRMM data are analyzed here only for 1 January through 31 August 1998, the period when the CERES scanner was operational. The TMI is a nine-channel, passive MW radiometer measuring radiances at frequencies of 10.65, 19.35, 21.3, 37.0, and 85.5 GHz. All channels have both vertically (V) and horizontally (H) polarized measurements except for the 21.3-GHz channel, which has only vertical polarization. TMI scans conically with an incident angle of 52.8° at the sea surface and yields a swath width of ~758.5 km. The 85.5- and 37-GHz effective footprints are 7 km (down-track direction) × 5 km (cross-track direction) and 16 × 9 km, respectively. The plane-parallel MW radiation transfer model of *Lin et al.* [1998a] was used to simulate brightness temperature Tb for all TMI channels. A lookup table was built for various atmospheric conditions including a range of cloud temperatures (Tw), LWP, atmospheric column water vapor (WV), near-surface wind speed (WS), and sea surface temperature (SST). For each cloudy pixel, LWP and Tw can be retrieved from the lookup table simultaneously using SST, WS, WV, and Tb_{37H} and Tb_{85V} measurements as in the work of *Ho et al.* [2003], hereafter denoted as HO3.

[7] The TRMM VIRS is a five-channel imager that measures radiances at 0.65 (VIS), 1.64, 3.75, 10.8 (IR), and 12.0 μm with a nominal 2-km spatial resolution. The VIRS cross-track scan yields coverage roughly between 38°N and 38°S. The VIRS radiance data were used to retrieve cloud fraction, thermodynamic phase (water or ice phase), optical depth, effective particle size, and water path (WP) as well as surface skin temperature, cloud-top temperature Tc,
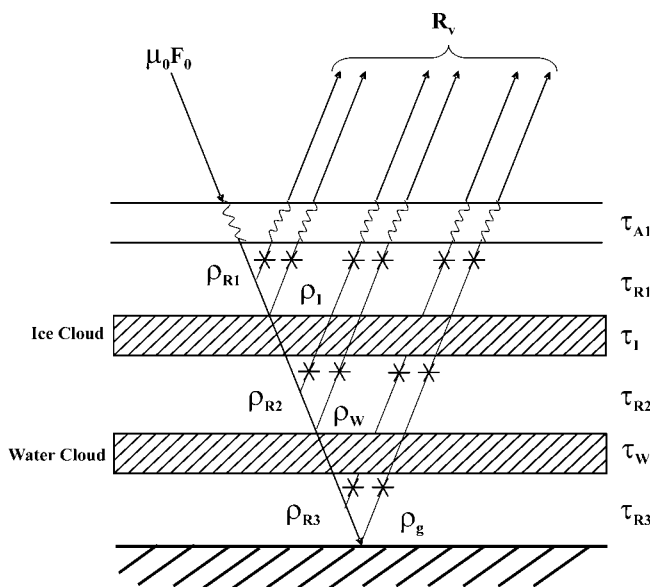
Figure 1. Schematic diagram of scattering and absorption processes for the two-layer cloud model.

and cloud-top height z for the CERES project [*Minnis et al.*, 1995, 2002]. Ice and LWP retrievals were calculated for each cloudy VIRS pixel using the cloud optical depth and effective particle size estimated with the VIS−IR Solar-IR Split-Window Technique (VISST) assuming a single cloud phase and layer for all clouds in the atmospheric column [*Minnis et al.*, 1995, 1998]. This study uses the same data sets and retrievals as HO3 except that the CERES TRMM Edition-2 VIRS cloud properties and spectral radiances [*Minnis et al.*, 2002] are used here instead of the Edition-1 cloud properties [*Minnis et al.*, 1999]. In addition to other changes, the Edition-2 algorithm uses a different VIS reflectance parameterization [*Arduini et al.*, 2002] and accounts for absorption of VIS wavelength radiation by WV. Relative to the Edition-1 retrievals, these two changes tend to reduce the optical depth for thin clouds, increase the optical depth for thicker clouds, and reduce the solar zenith angle (SZA) dependence of the optical depth retrievals.

[8] Since TMI has much larger footprints (∼20 km) than VIRS, the VIRS cloud products were convolved with TMI measurements to produce equivalent VIRS cloud retrievals within the TMI footprints. Only the TMI pixels containing more than 15% cloudiness from the convolved VIRS–TMI data are used here. The resulting data set constitutes 81.6% of all TMI pixels taken over the oceans. Because TMI and VIRS are on the same spacecraft, the temporal and spatial mismatches of VIRS and TMI measurements are negligible. The detailed collocation and retrieval processes for the TRMM data can be found in HO3.

3. Methodologies

3.1. Two-Layer Model and Retrieval Algorithm

[9] A cloud AD radiation transfer model [*Minnis et al.*, 1993] is used to characterize the reflectance fields for multilayered clouds. The upper and lower layers consist of ice particles and water droplets, respectively. Ice particle effective diameter is denoted as De and defined as in the

work of *Minnis et al.* [1998]. To distinguish between water and ice clouds, the effective droplet radius is denoted as r_e and is the ratio of the integrated droplet volumes to the integrated cross-sectional areas over the entire size distribution. Figure 1 shows the schematic diagram of scattering and absorption processes for this simple two-layer cloud AD model. The multiple reflection and transmission between the two cloud layers as well as the counterparts between the clouds and the surface are taken into account by the forward radiative transfer computations. The 0.65-μm reflectance R_v at particular solar zenith (θ_0), viewing zenith (θ), and relative azimuth (ψ) angles (Table 1) were computed with the AD model using 11 ice cloud models and 7 water cloud models [*Minnis et al.*, 1998] for ice cloud optical depths τ_I ranging from 0 to 128 and water cloud optical τ_W ranging from 0 to 32. Three scattering layers, $i = 1, 2, 3$, with reflectances ρ_{Ri} and Rayleigh optical depths τ_{Ri}, are separated by the two cloud layers and sandwiched between an ozone absorption layer and a surface with reflectance ρ_s. The incoming radiation is indicated in Figure 1 as the spectral solar constant F_o multiplied by $\mu_o = \cos \theta_o$. The computed values of R_v were compiled in type-specific lookup tables. For the lookup tables, the high cloud was placed at 200 hPa and the water cloud was located at 900 hPa. The ozone absorption is computed in the highest layer of the model using an optical depth, τ_{A1} of 0.0332, a value corresponding to the average, 0.32 cm (at standard temperature and pressure), for the midlatitude summer and winter standard atmospheres of *McClatchey et al.* [1973]. Changing the upper and lower cloud pressures by 200 hPa resulted in reflectance differences of less than 1%. The largest reflectance differences occur for $\tau_I < 4$ with $\tau_W < 1$, a case that is unlikely to be discerned with the MCRS. The error range for the remaining combinations was generally smaller than ±0.5%. Thus there is only minimal impact using fixed cloud pressures for the retrievals.

[10] The reflectances for any set of angles, optical depths, and lower-cloud r_e are estimated from the lookup tables using nearest-node values and interpolations with combinations of linear and Lagrangian methods as in *Minnis et al.* [1998]. Given the LWP and r_e of the lower-layer water cloud, a set of TOA VIS reflectances can be easily computed using these lookup tables of reflectance for each optical depth node and ice particle size.

[11] Examples of reflectances from combined cloud layers are given in Figures 2 and 3. Figure 2 shows ρ at $\theta_0 = 45°$ as a function of viewing and illumination angles

Table 1. Summary of Zenith Angles and Optical Depths Used for Multilayered Cloud Reflectance Lookup Tables Computed With the Adding-Doubling Radiative Transfer Model

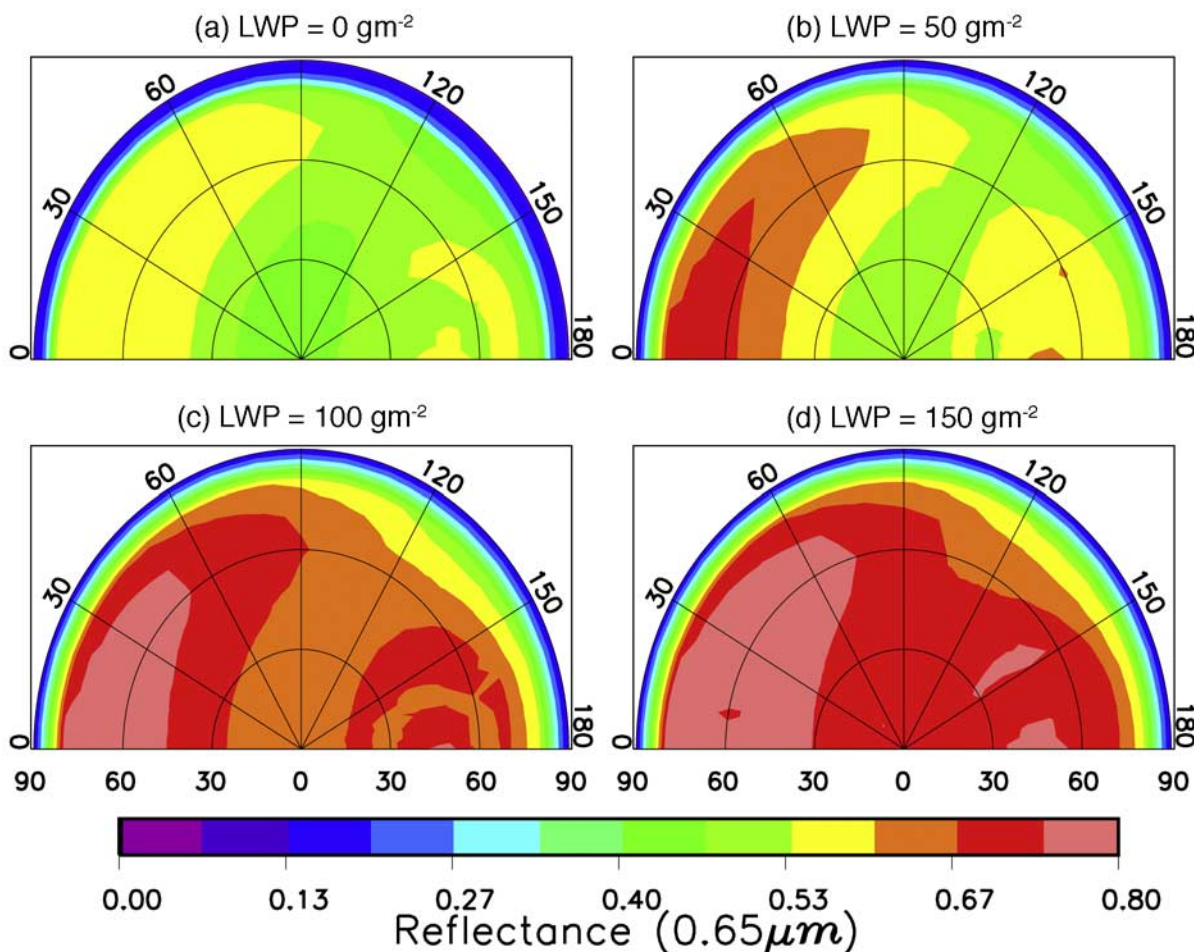|	
θ_0, θ	0.0, 18.19, 25.84, 31.78, 36.87, 41.41, 45.57, 49.4653.13, 56.63, 60.0, 63.27, 66.42, 69.51, 72.54, 75.52, 78.46, 81.37, 84.26, 87.13, 90.0
ψ	0.0, 2.5, 5.0, 10, 15, 25, 35, 45, 55, 65, 75, 85, 95, 105, 115, 125, 135, 145, 155, 165, 175, 180
τ_I	0.0, 0.25, 0.5, 1, 2, 3, 4, 8, 16, 32, 64,128
τ_W	0.0, 0.10, 0.20, 0.30, 0.40, 0.50, 0.60, 0.70, 0.80, 0.90, 1.00, 1.20, 1.40, 1.60, 1.80, 2.00, 2.50, 3.00, 3.50, 4.00, 5.00, 7.50, 10.0, 15.0, 20.0, 25.0, 30.0

Figure 2. Combined ice and water cloud VIS reflectances at $\theta_o = 45°$ and IWP = 160 g m^{-2} as functions of θ (radial) and ψ (circular) coordinates.

from the AD calculations using a fixed upper-layer ice cloud optical depth ($\tau_I = 8$) and effective ice crystal diameter (De = 67 μm) that yields IWP = 160 g m^{-2} over water clouds with four different LWPs. R_v increases and becomes more isotropic as LWP rises from 0 to 150 g m^{-2}.

[12] The anisotropy is different, however, from that expected for a pure ice cloud with the same albedo. The anisotropic difference and reflectance increase cause the VISST retrievals to overestimate IWP and TWP when a lower cloud is present due to the one-layer assumption. Figure 3 shows R_v for the same conditions except that the TWP is fixed at 200 g m^{-2} and LWP and IWP are varied as indicated in the plots. Figures 2a and 3a are similar in pattern because both have no water influence. However, Figures 2c and 3d are also quite similar despite the former having a value of TWP that is 60 g m^{-2} greater than that in the latter plot. These plots illustrate the importance of properly treating the reflectance field in multilayered conditions. For example, in Figure 2c, at $\theta = 60°$ and $\psi = 45°$, $R_v = 0.74$. An SL ice cloud with the same TWP would produce $R_v = 0.65$. A retrieval based on R_v for the cloud system in Figure 2c using the assumption that the entire cloud is ice phase would yield IWP = TWP = 345 g m^{-2}. In

this case, the retrieved IWP and TWP are overestimated by 245 and 145 g m^{-2}, respectively.

[13] Figure 4 shows the variation of TOA diffuse albedo A_v as a function of τ_I and τ_w. The diffuse albedo is significantly impacted by lower-layer water clouds and is especially sensitive to their optical depth τ_w. For a given value of A_v, τ_I for an OL cloud ($\tau_w > 0$) should be smaller than τ_I for an SL ice cloud. For example, if $A_v = 0.6$, the case with $\tau_w = 0$ yields $\tau_I \approx 12$, but if $\tau_w = 10$, $\tau_I \approx 5$. Very similar results are found with the other ice models (not shown here). It is clear that as τ_w increases, the sensitivity to changes in τ_I decreases so that estimates of τ_I when $\tau_I < 2$ are more uncertain than those for thicker high clouds. The values of A_v for different ice cloud models at $\tau_w = 2$ and $r_e = 12$ μm in Figure 5 vary by as much as 0.1 ($\tau_I = 10.0$) for differing ice cloud particle diameters. For a given albedo, τ_I varies by as much as 35% depending on the value of De. The sensitivity of TOA diffuse albedos to varying r_e at $\tau_w = 30$ and De = 30.36 μm is shown in Figure 6. For a range of r_e between 4 and 32 μm, A_v varies by 0.05 for $\tau_I = 0.25$ and by 0.03 for $\tau_I = 10$, approaching zero at larger values of τ_I. If only values of r_e between 8 and 32 μm are considered, however, the A_v range is generally only 0.02 or less. Since the average
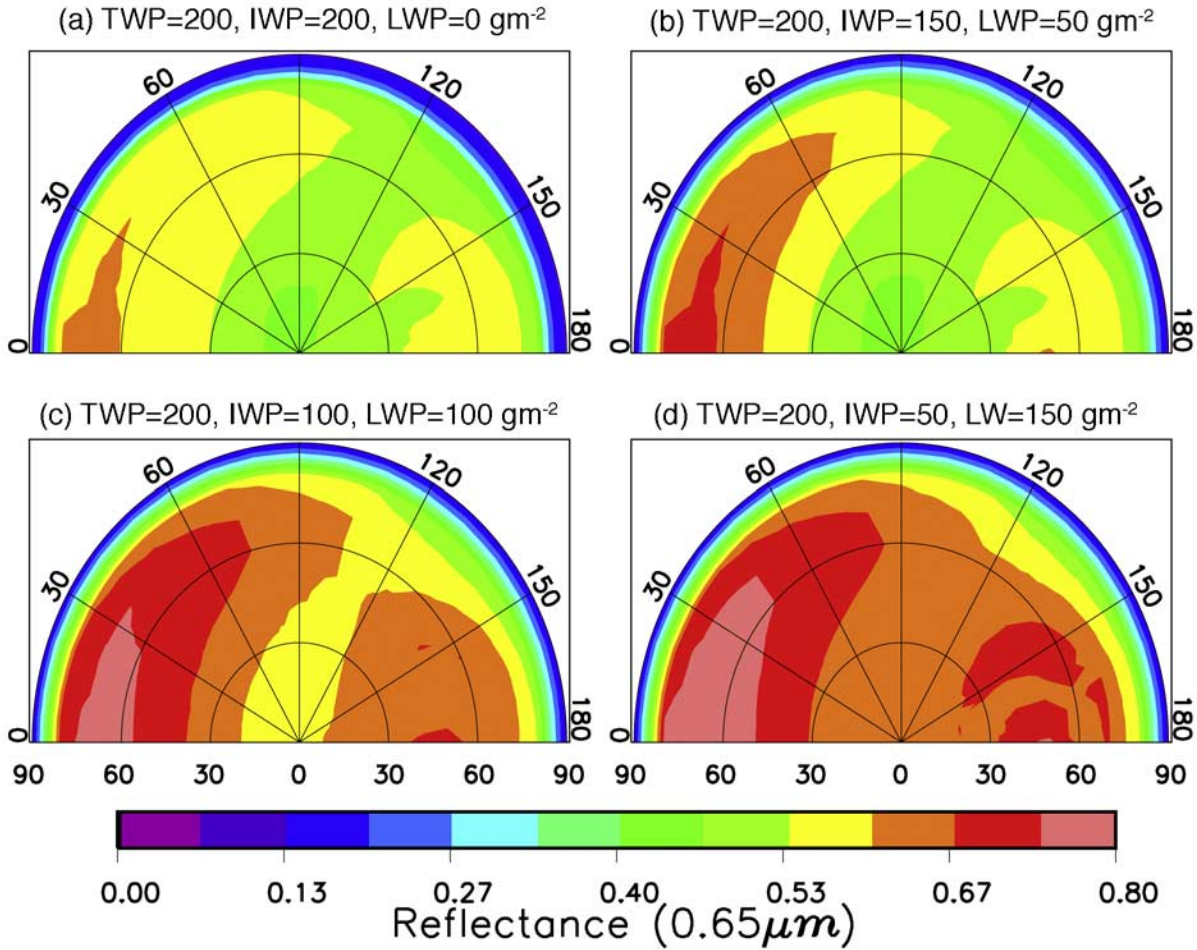
Figure 3. Same as Figure 2 but for fixed TWP, and variables IWP and LWP.

value of r_e is typically between 9 and 18 μm over ocean areas [e.g., *Minnis et al.*, 2002], the variations in r_e should not have a significant impact on the derived IWP for most cases. Similar results are expected for the bidirectional reflectances because the angular reflectance patterns of SL low clouds vary minimally for a given optical depth as seen in Figure 5 of *Minnis et al.* [1998].

[14] To improve the accuracy of ice cloud property retrievals, an updated MCRS is developed that is radiatively consistent with the derived water paths. Initially, the SL VISST retrieval is used to detect cloudy pixels and estimate the cloud properties by treating each cloudy pixel as a *single-layered* cloud. Next, the combined MW, VIS, and IR (MVI) method [*Lin et al.*, 1998a, 1998b] is used to detect OL cloudy pixels. The MVI technique detects overlapping clouds by using the difference between Tw retrieved from TMI MW data and the cloud effective temperature (Tc) derived from VISST [*Lin et al.*, 1998b]. The third step is to estimate the optical depth of the lower-layer water cloud. Following *Minnis et al.* [1998], the optical depth of the lower-layer water cloud can be written as

$$\tau_w = 0.75 \ Q_{vis}(r_e)LWP/r_e, \qquad (1)$$

where

$$r_e = r_0 + r_1 * LWP, \qquad (2)$$

and $Q_{vis}(r_e)$ is the extinction efficiency for a given effective droplet radius. For the ocean, $r_0 = 12$ and $r_1 = 0.0186$. Equation (2) was derived from the statistics of SL water clouds based on 8 months of CERES VIRS-based SL
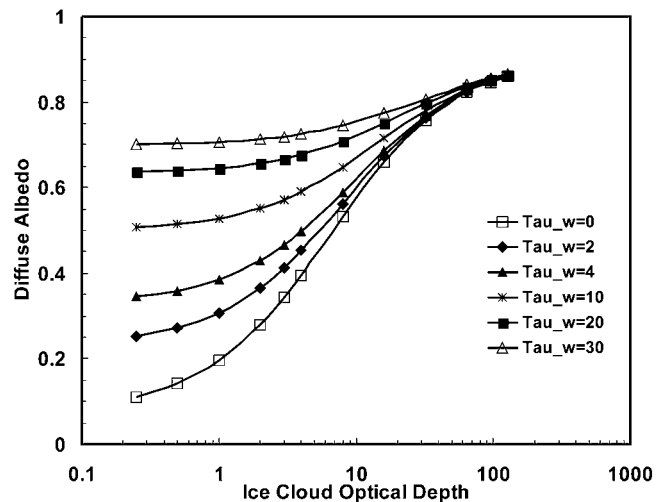

Figure 4. Variation of diffuse albedo with τ_I for CS ice model (De = 41 μm) for range of lower-layer water cloud optical depths.
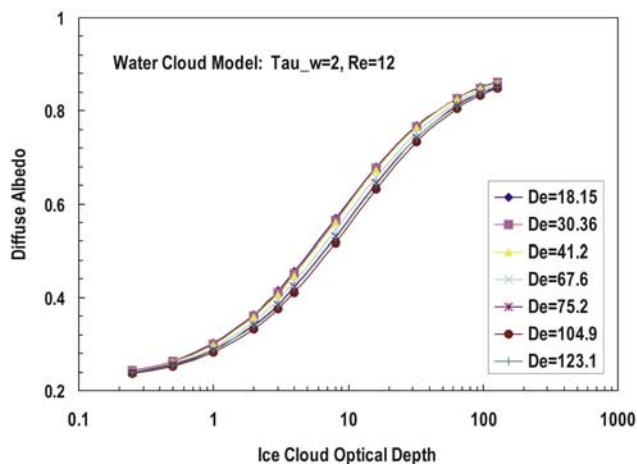
Figure 5. Variation of TOA diffuse albedo with ice cloud optical depth for different ice models and lower-layer water cloud having $\tau_w = 2$ and $r_e = 12$ μm.

VISST cloud retrievals [*Minnis et al.*, 2002]. Thus, given the MW LWP, the values of r_e and τ_w are computed with equations (1) and (2) and then used to select the proper lookup tables. TOA radiances are then computed for every combination of the specified low-level cloud and the upper-layer ice cloud. In formulation, the MCRS retrieval follows the iterative VISST procedure resulting in recalculation of the effective ice crystal diameter De, τ_I, and IWP for the upper-layer cloud. In this study, the value of De found from the initial VISST retrieval is assumed to be valid for the upper-layer cloud. Therefore the MCRS only needs to match the two-layer cloud lookup table reflectances to the observed reflectances for the given viewing and illumination angles, τ_w, and De. In all cases, the surface albedo is set to 0.04, a value close to the diffuse surface albedo at

0.64 μm. Since relatively thick two-layer cloud systems are being analyzed here, the diffuse albedo approximation should apply for the OL cases. The VISST used for the SL cases employs a variable surface reflectance field.

[15] The uncertainty in LWP derived from the satellite MW measurements is ±40 g m^{-2} [*Lin et al.*, 1998a, 1998b]. On the basis of that uncertainty, *Huang et al.* [2005] found that, overall, the ice cloud properties are more sensitive to underestimates in LWP than to overestimates. The optical depth increases by about 10% for LWP underestimated by 40 g m^{-2} compared to only a 2% decrease for a 40 g m^{-2} overestimate in LWP. The value of De is only affected by ±2%, whereas the LWP uncertainty translates to an uncertainty of −7.6 to +3% in IWP. The sensitivity is larger for smaller values of IWP.

[16] The assumption that the value of De from the SL VISST can be used for the upper-layer ice cloud also causes some uncertainty in the retrievals. The exact error in De and IWP resulting from using the SL ice crystal size depends on the viewing and illumination conditions, the actual sizes of the ice crystals and water droplets, and the value of τ_w. From the data of *Huang et al.* [2005], it is estimated that this approach can result in an error in De and, subsequently, IWP that ranges from roughly −40% at $\tau_I = 0.25$ to zero around $\tau_I = 6$ and up. The iterative retrieval of De sometimes yields a smaller value than the SL VISST result. Assuming the De error depends linearly on log(τ_I) from the results of *Huang et al.* [2005] for De = 60 μm, the IWP would be 2.7, 4.6, 5.5, and 5.5 g m^{-2} too low for $\tau_I = 0.25$, 1, 2, and 3, respectively, if the SL VISST value of De is used in the MCRS. Overall, the retrieval errors are small when using this assumption to simplify the MCRS.

3.2. OL Cloud Detection

[17] The value of Tw retrieved from TMI data represents the mean cloud water temperature of the integrated cloud column, whereas Tc derived from the VIRS data represents
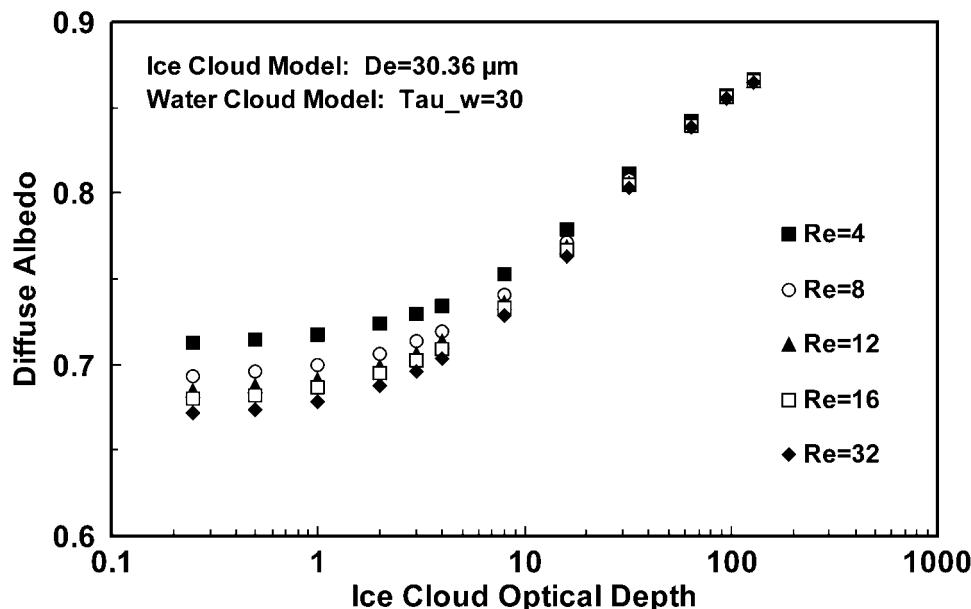

Figure 6. Variation of TOA diffuse albedo with τ_I for different r_e at $\tau_w = 30$ and De = 30.36 μm.
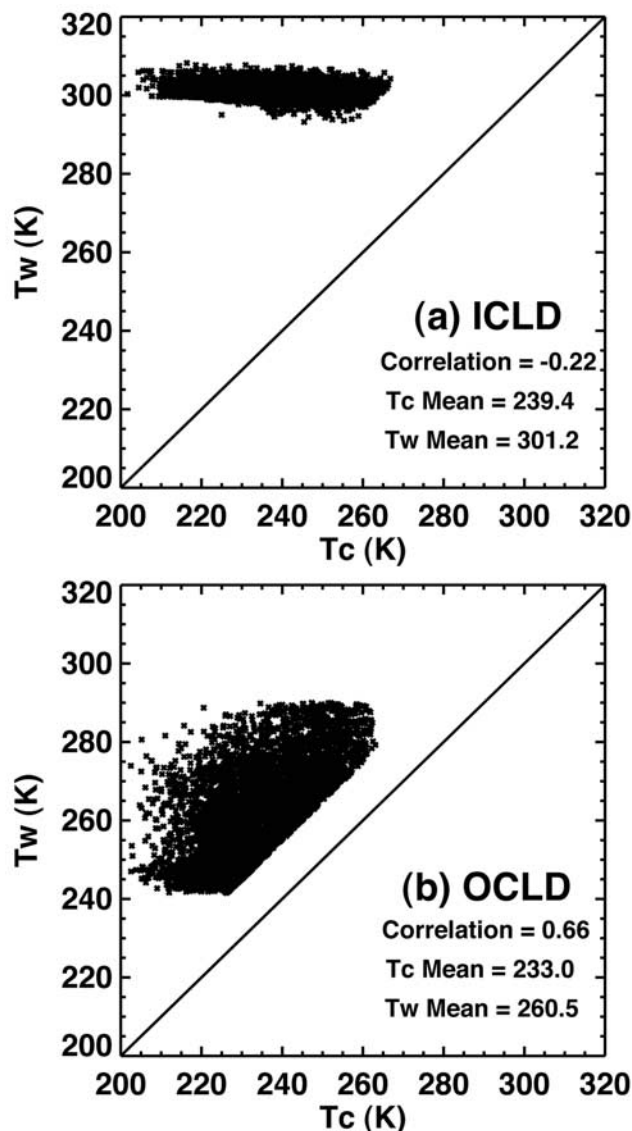
Figure 7. Variation of TMI Tw with VIRS Tc over tropical oceans during July 1998 for (a) single-layered ice clouds (ICLD) and (b) overlapped ice clouds (OCLD).

the temperature near the top of the cloud for optically thick clouds [*Minnis et al.*, 1993]. Therefore, when the difference, $\Delta Twc = Tw - Tc$, is significantly positive, it is highly likely that the observed system consists of OL clouds [*Lin et al.*, 1998b] or, at a minimum, of an ice cloud contiguous with an underlying water cloud. In this study, two special overcast groups are selected and studied. The conditions for selecting the two groups are as follows:

[18] (1) SL high ice clouds (ICLD): 100% ice phase, LWP < 40 g m^{-2}, Tw > 290 K, Tc < 273 K, |Ts − Tw| < 5 K, and Ts − Tc > 36 K, where Ts = SST.

[19] (2) OL clouds (OCLD): 100% ice phase, Tw < 290 K, Tc < 273 K, Tw − Tc > 15 K, Ts − Tc > 36 K, and LWP > 0 g m^{-2}.

The thermodynamic (ice/water) phase of the highest cloud was determined by the CERES VIRS analysis [*Minnis et al.*, 2002]. The thresholds used here exclude a significant portion of the overcast cloud data including mixed and liquid water phase clouds as well as ice clouds that are classified as precipitating so that LWP cannot be retrieved using the MW technique.

[20] The technique will sometimes miss OL clouds when the ice cloud is optically thin and the SL VISST classifies the scene as liquid water. In general, the CERES phase classifier will determine that the OL scene is an ice cloud whenever $\tau_I > 0.75$ or so. For smaller ice cloud optical depths, the scene will be classified as an ice or liquid water cloud depending on several variables such as the viewing and illumination angles, the sizes of the ice crystals and water droplets, and the value of τ_w. As seen later, the phase classifier can detect some OL scenes for values of τ_I as low as 0.15, but it is clear that some OL clouds with $\tau_I < 0.75$ are not analyzed because the phase was determined to be liquid water for the SL case.

4. Results

[21] Only ice-over-water clouds are the focus of this study. The OCLD and ICLD groups together constitute about 13.5% of all overcast cases and half of all VIRS pixels classified as ice phase using the initial VISST analysis. The remainder of the ice phase clouds are either in the precipitating or fractionally cloudy categories. The average ice cloud coverage for the entire domain is 19.3%.

4.1. OL Cloud Amounts

[22] Figure 7 shows scatterplots of Tw with Tc for each of the two groups for tropical ocean (20°S–20°N) regions during July 1998. The relationships between Tw and Tc are distinct for each group. For SL ice clouds in Figure 7a, Tw is very narrowly distributed around 300 K. In contrast, Tc is very low, ranging from 210 to 265 K with a mean of 239.4 K and a standard deviation of 12.1 K. In the ICLD case, there is almost no liquid cloud water in the atmosphere (LWP ∼ 0), and the TMI radiances are directly from the sea surface with some attenuation by atmospheric WV and other trace gases. Thus, the estimated Tw values are not really cloud water temperatures; instead, they are more representative of the SST. The negative linear correlation coefficient ($R = -0.22$) between Tw and Tc further demonstrates a relationship between Tw and SST. Fewer SL cirrus clouds occur over the colder waters of the Tropics where low-level clouds and subsidence predominate.

[23] The OL cloud systems (OCLD) have a strong positive correlation between Tw and Tc (Figure 7b). The mean Tw (260.5 K) is about 27.5 K greater than the average Tc values (233.0 K), although the standard deviations, 11.3 and 12.5 K, respectively, are similar. In addition to the presence of OL clouds, this large difference arises from the fact that the MW radiation emanates from much lower cloud layers than the IR radiances measured by VIRS. This result confirms that significant differences between Tw and Tc can be used as the critical condition for identifying cloud overlap.

[24] The frequency distributions of OL clouds for July 1998 over the domain ocean areas are shown in Figure 8 as functions of two parameters derived from the TMI. The frequency of occurrence (FOC) is defined as the percentage of OL clouds in a given parameter bin relative to the total number of OCLD pixels. More than 70% of the lower-layer clouds (Figure 8a) are relatively thin water clouds with LWP
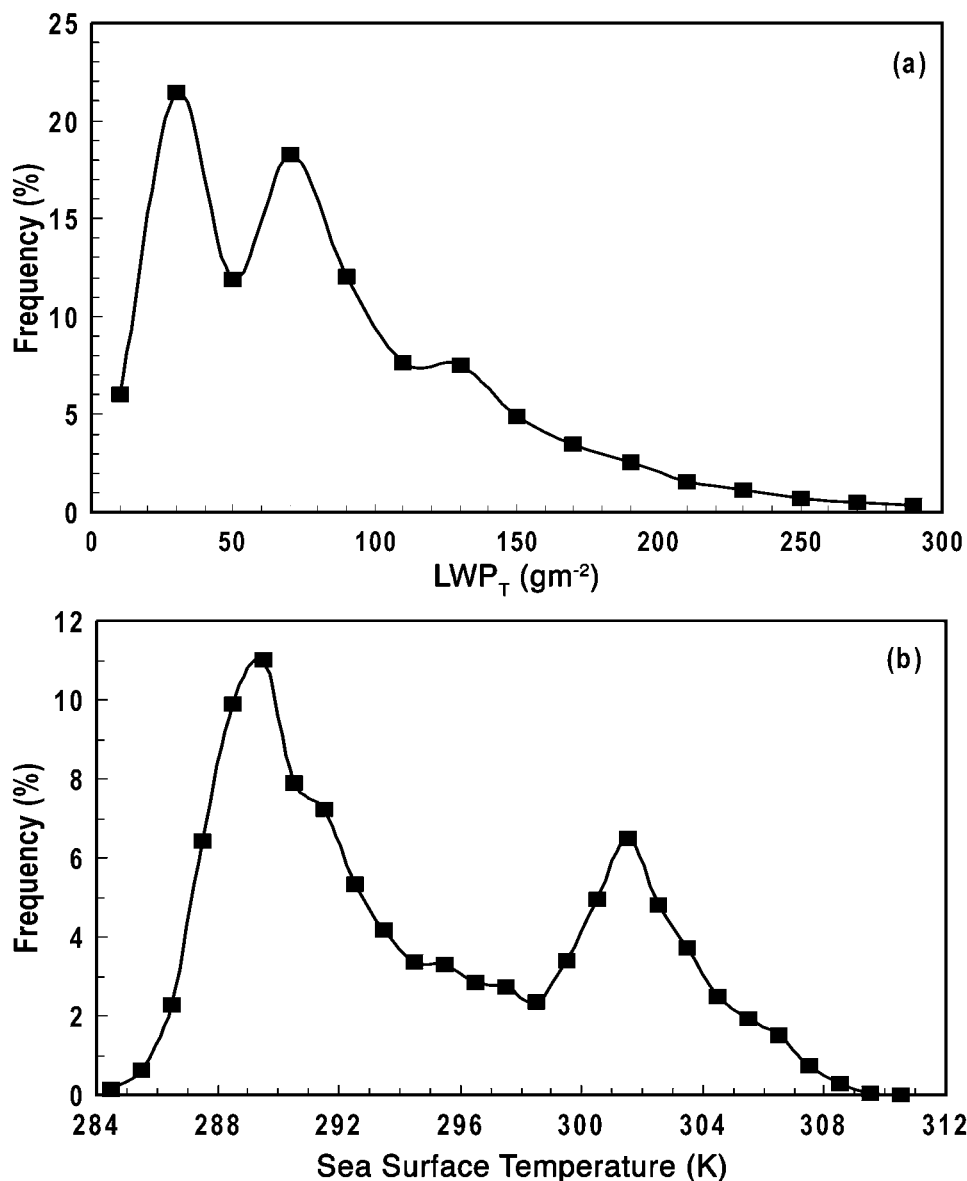
Figure 8. Overlapped cloud frequency of occurrence over water surfaces (38°S–38°N) during July 1998 as functions of (a) TMI LWP and (b) SST.

< 100 g m^{-2}; LWP peaks at 30 and 70 g m^{-2}. OCLDs occur most often when SST = 289.5 K (Figure 8b), whereas a secondary peak is seen at 302 K. More than 55% of OCLD pixels are found in regions with SST < 295 K.

[25] Figure 9 shows the FOC variations of three OCLD types for different zonal bands from January through August 1998. The occurrence frequency is defined as the percentage of the overlap type relative to the total number of OCLD pixels. These three types are (1) ice-over-warm-water cloud systems (IOWW), where Tw > 273 K; (2) ice-over-supercooled water cloud systems (IOSW), where $255 <$ Tw < 273 K; and (3) ice-over-extremely-super-cooled water clouds (IOEW) with Tw < 255 K. For IOSW and IOEW, the lower-layer clouds may consist of a mixture of both ice and water particles, whereas both thin cirrus and thick anvils can comprise the upper-layer clouds. The deepest convective clouds are likely to be confined to the IOEW category. The IOSW clouds (dotted

curves) are the major type of ice-over-water cloud systems in all regions, accounting for more than 55% of all OCLD pixels compared to 15 and 30% for IOEW (dashed) and IOWW (solid), respectively. These results are consistent with ship observations [*Hahn et al.*, 1982], which show that in the Tropics, cirrus clouds overlap altostratus, cumulus, and cumulonimbus more often than they occur over stratus and stratocumulus.

[26] Globally between 37°N and 37°S, the FOCs of the three OCLD types vary minimally with season (Figure 9a). IOEW increases by ∼8% from January to August, whereas IOSW decreases by a similar amount. The most striking seasonal changes occur between 20°N and 37°N (Figure 9b), where IOSW drops by 20% as IOEW doubles from 25% from winter to summer. IOWW peaks in April and falls to a minimum during summer. Presumably, the seasonal rise in IOEW is linked to increased deep convection during summer. Deep convection should
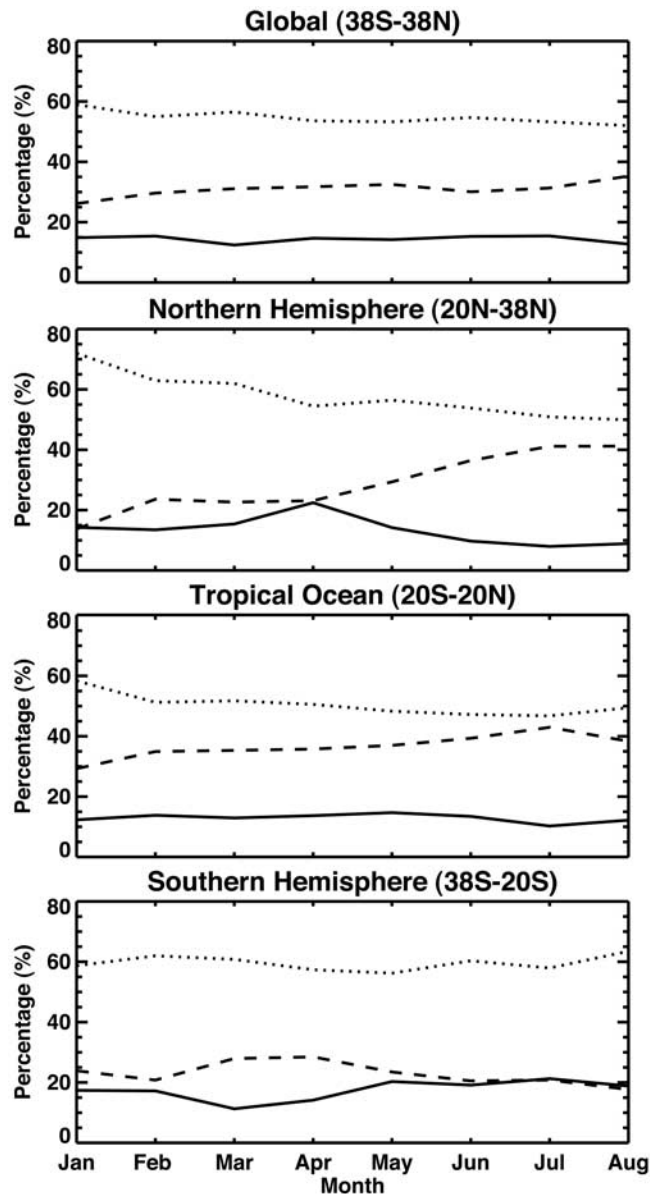
Global (38S-38N)

Northern Hemisphere (20N-38N)

Tropical Ocean (20S-20N)

Southern Hemisphere (38S-20S)

Figure 9. Seasonal variation of occurrence frequencies for ice-over-warm-water (IOWW, solid), ice-over-supercooled-water (IOSW, dotted), and ice-over-extremely-supercooled-water (IOEW, dashed) clouds from January to August 1998.

raise liquid water up to greater altitudes underneath anvil-produced cirrus than that generated by baroclinic disturbances, which are more common in other seasons and produce many layers of water clouds beneath cirrus shields. A similar convergence of the IOSW and IOEW occurs in the Tropics (Figure 9c) during the boreal summer when the intertropical convergence zone (ITCZ) is most developed. The seasonal variability in the three OCLD types is least in the southern subtropics where IOEW and IOWW are of the same magnitude.

4.2. Cloud Properties

[27] The cloud properties from each category and analysis type were averaged for each month and season and plotted

only for the area between 30°S and 30°N to minimize the impact of sampling noise that occurs at the higher latitudes. Figure 10 shows the mean values of De during June–August (JJA) 1998 for the ICLD VISST retrievals and the OCLD MCRS retrievals. Since the iteration to recalculate De was not used here in the MCRS, the values for OCLD are same for both the VISST and the MCRS analyses, so the former is not shown. These results indicate that De for the OCLD cases is similar to but slightly larger than the ICLD values. Similar results were found for the other two seasons, January–February (JF) and March–May (MAM), as seen in Table 2. The mean values of De for all seasons combined are 61.6 and 58.6 μm for the ICLD and OCLD cases, respectively.

[28] VISST optical depths for all ice clouds during JJA generally range from 0.5 to 32 with a few scattered regions with $\tau_I > 32$ (Figure 11a). If only the OCLD cases are considered (Figure 11b), the bottom end of the range is increased up to 2 or 3, whereas many new regions have means exceeding 32. The thickest clouds are probably excluded from the OCLD category because of precipitation, whereas the thinnest clouds are unlikely to be OL. The mean value of τ_I in Figure 11b is 19.2. Most of the overcast ice clouds without significant liquid water beneath them (ICLD, Figure 11c) have $\tau_I < 16$ with some extremely low mean values ($\tau_I < 0.5$) off the coast of Brazil. The largest values are seen off the coasts of southern Asia and eastern Australia and in the Gulf of Mexico. Overall, $\tau_I = 9.6$. Application of the MCRS to the OCLD cases (Figure 11d) substantially reduces the number of regions with $\tau_I > 16$ and raises the number of areas with $\tau_I < 8$ resulting in an average optical depth of 11.3. This represents a 59% reduction in τ_I for the OCLD cases. Instead of being twice as thick as their SL counterparts, the MCRS reveals that the OL ice clouds detected here are only 11% thicker, on average, than the ICLDs. These results are typical for all seasons as indicated in Table 2.

[29] Combining τ_I and De yields IWP, which is plotted for the various algorithms in Figures 12 and 13 for JF and JJA, respectively. For all of the ice clouds retrieved with the VISST (Figures 12a and 13a), the monthly means range from less than 4 g m^{-2} in the subsidence zones to over 1024 g m^{-2} in a few areas. The range in the means for the OCLD subsets (Figures 12b and 13b) of the total VISST retrievals is narrowed with the minimum between 64 and 128 g m^{-2} during both seasons. The ICLD optical depths (Figures 12c and 13c) vary over the same range as the total VISST retrievals. The largest values occur over the Caribbean during winter and in the southern Indian Ocean during boreal summer. The MCRS decreases IWP for the OCLD cases (Figures 12d and 13d) to values that are more like the ICLD values than the VISST OCLD results. The maximum values, found mainly in the ITCZ in both figures, do not exceed 1024 g m^{-2}. The differences between the VISST and MCRS OCLD cases, shown in Figures 12e and 13e, are all positive and mostly greater than 200 g m^{-2} in the ITCZ. Seasonally, the mean VISST OCLD IWP ranges from 355 g m^{-2} in winter to 393 g m^{-2} in summer (Table 2) with a mean of 370 g m^{-2}, 157 g m^{-2} greater than the MCRS IWP. The MCRS OCLD IWP also peaks in summer, whereas the mean ICLD IWP remains relatively constant over the 8-month period. The former is less than 7%
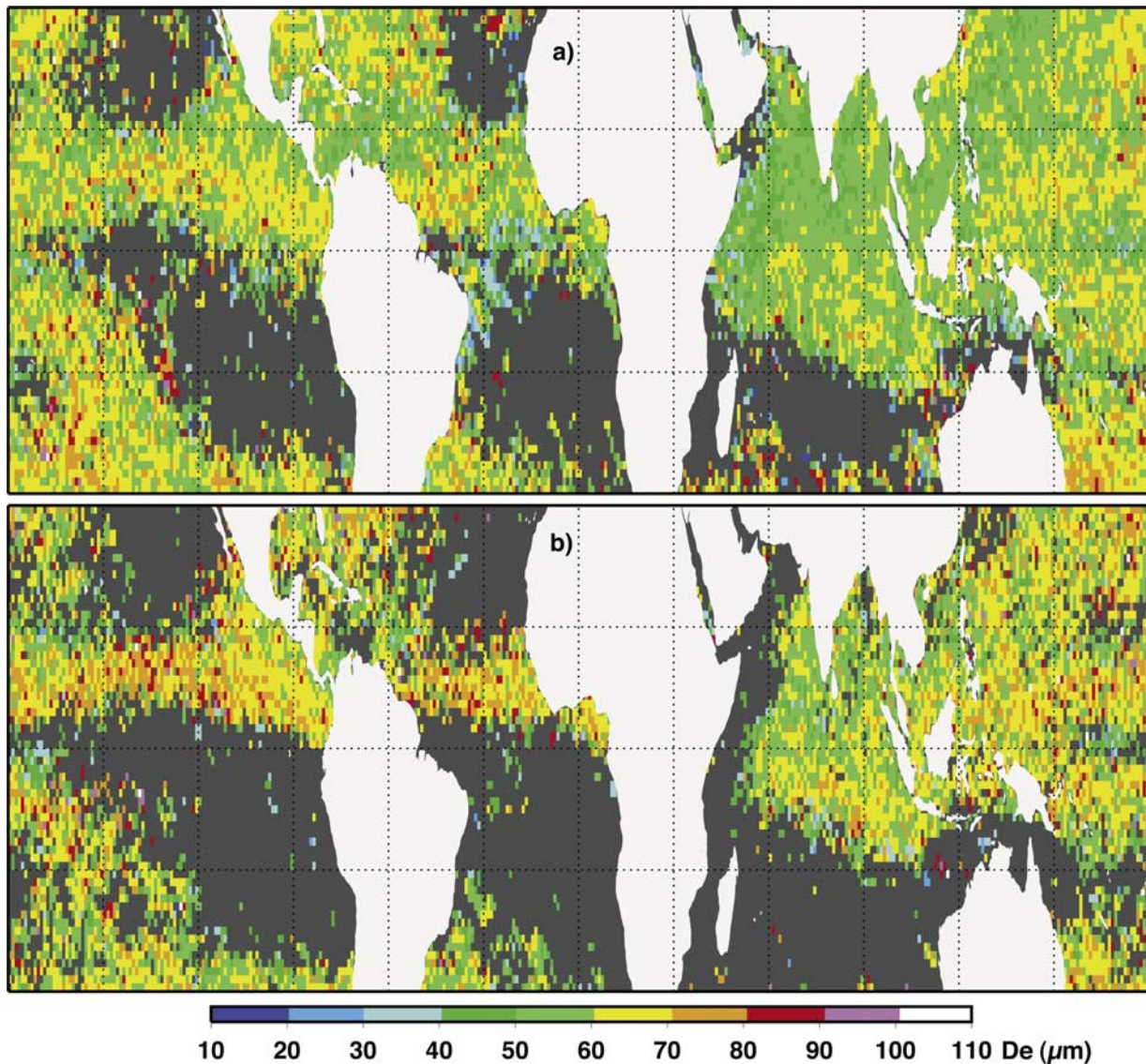
Figure 10. Mean effective ice crystal diameter for (a) VISST single layer and (b) MCRS overlapped overcast ice cloud TMI pixels over water between 30°S and 30°N, June–August 1998.

greater than ICLD IWP, on average, and 42% less than its VISST counterpart.

5. Discussion

5.1. Comparisons to Radar Estimates of IWP

[30] Validation of this retrieval method is difficult because reliable independent estimates of IWP in OL clouds are limited to retrievals using cloud radar data or in situ data. The latter are quite rare and do not provide robust statistics; thus the radar option is the most feasible approach. Earlier studies of SL ice clouds showed that the VISST yields quite reasonable estimates of IWP compared to radar-based retrievals [e.g., *Mace et al.*, 2005]. Most cloud radar data are taken over

Table 2. Seasonal Mean Ice Cloud Properties for Overcast Ice Cloud TMI FOVs Over Water, 30°S–30°N, 1998

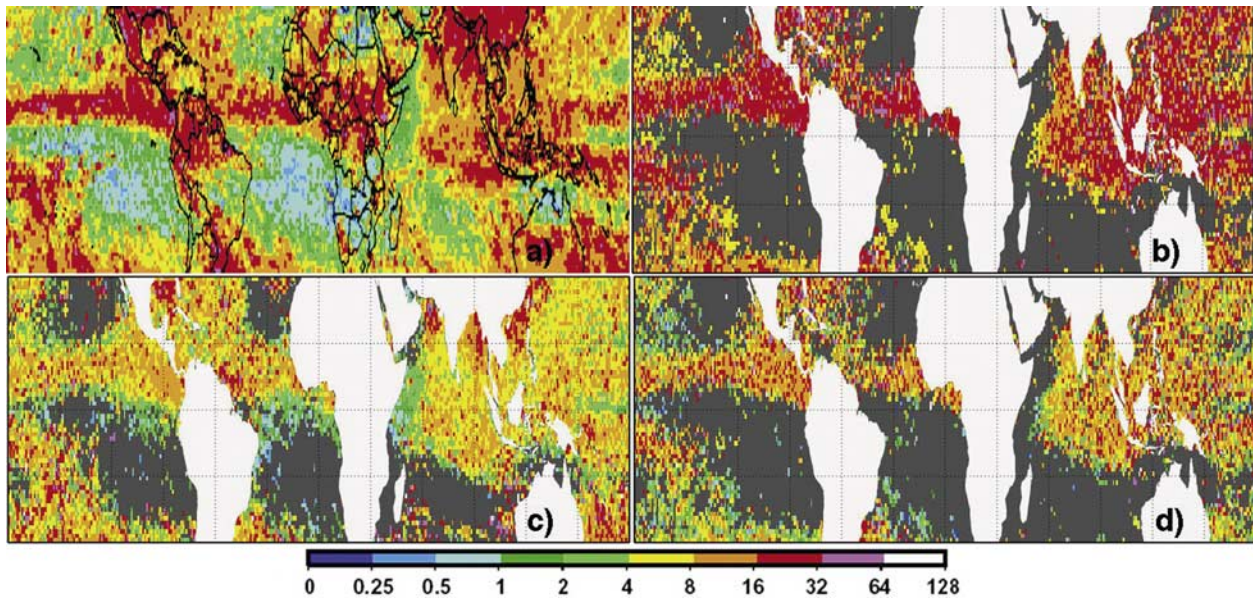| Parameter	JF	MAM	JJA	8-mo. Mean
OCLD MCRS, De, micrometers	61.2	61.5	62.2	61.6
ICLD VISST, De, micrometers	58.1	59.0	58.6	58.6
OCLD VISST, τ	17.5	17.6	19.2	18.1
OCLD MCRS, τ	10.2	10.1	11.3	10.5
ICLD VISST, τ	9.4	9.5	9.6	9.5
OCLD VISST, IWP, grams per square meter	355	359	393	370
OCLD MCRS, IWP, grams per square meter	205	206	229	213
ICLD VISST, IWP, grams per square meter	200	200	201	200

Figure 11. Cloud optical depths from VIRS, June–August 1998. (a) All ice clouds from VISST analysis. (b) Ice clouds from VISST analysis identified as overlapped (OCLD) by MVI. (c) Ice clouds identified as single-layered (ICLD) by MVI. (d) Same as (b) except from MCRS analysis.

land where the satellite-borne MW radiometer yields unreliable measurements of LWP. However, uplooking surface-based MW data can substitute for the TMI measurements.

[31] Preliminary assessment of the MCRS IWP is accomplished by comparison with simultaneous retrievals from the Millimeter Cloud Radar (MMCR) at the Atmospheric Radiation Program (ARM) Southern Great Plains Central
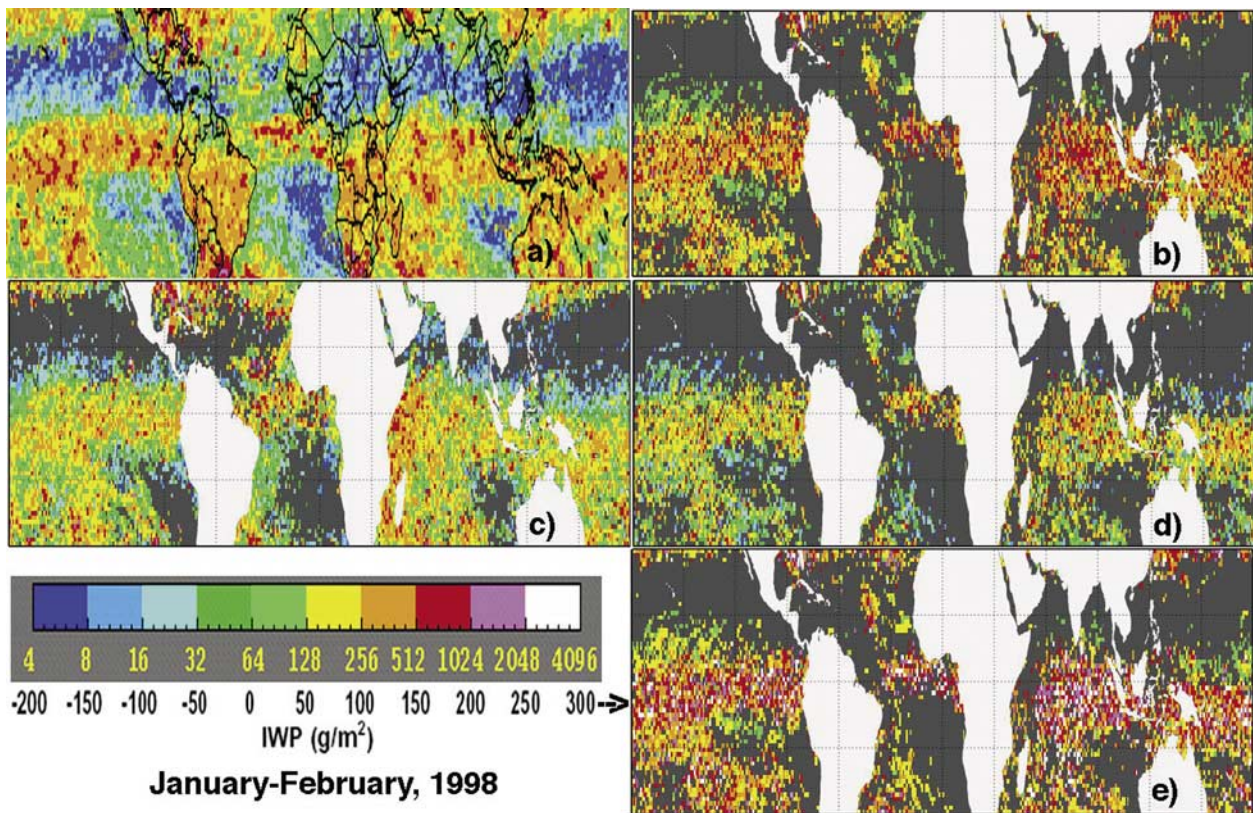

Figure 12. Cloud IWP from VIRS, January–February 1998. (a) All ice clouds from VISST analysis. (b) Ice clouds from VISST analysis identified as overlapped (OCLD) by MVI. (c) Ice clouds identified as single-layered (ICLD) by MVI. (d) Same as (b) except from MCRS analysis. (e) Difference between OCLD analyzed with (b) VISST and (d) MCRS.
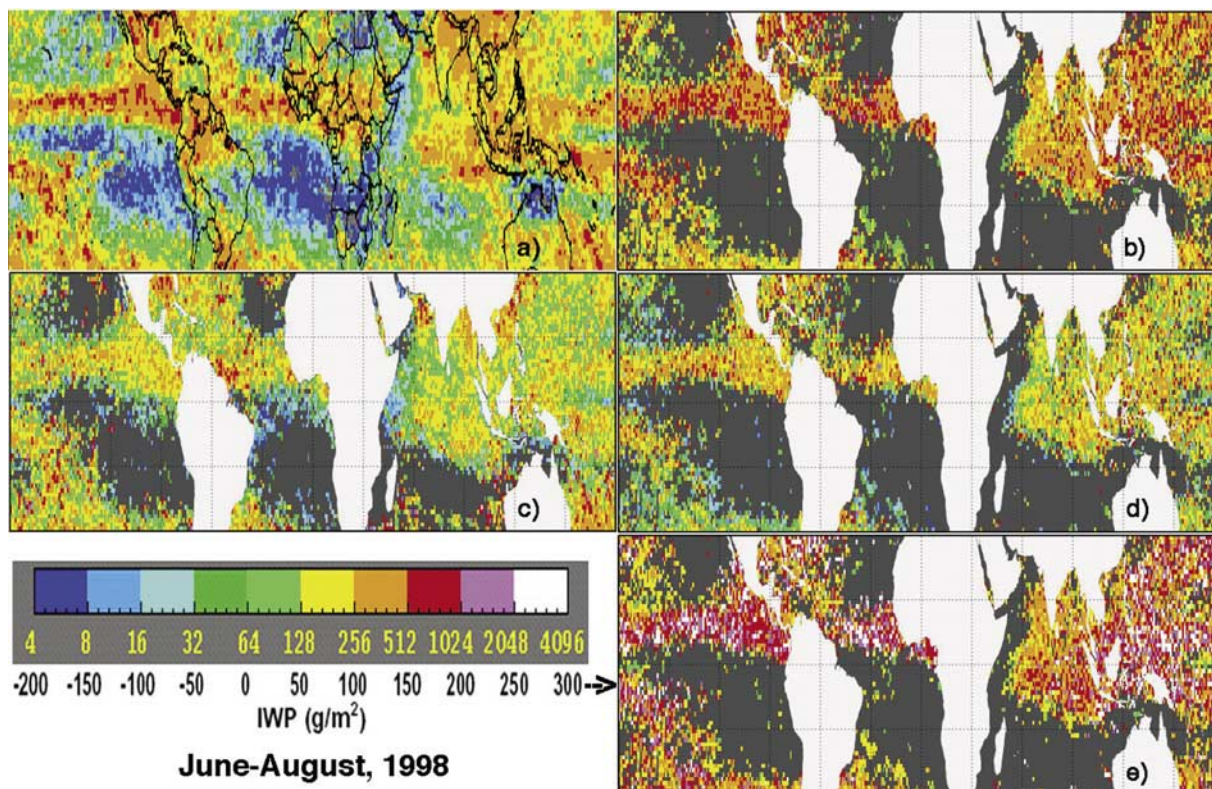
Figure 13. Same as Figure 12 except for June–August 1998.

Facility (SCF) in Oklahoma. The 10 cases of ice-over-water clouds for 3 days in 2000 used by *Huang et al.* [2005] are also employed here for comparison. These cases cover a wide range of viewing, illumination, and scattering angles. Figure 14 compares the IWP derived from the Eighth Geostationary Operational Environmental Satellite (GOES-8), which substitutes for VIRS, and surface-based MW data using the MCRS, from using VISST [*Minnis et al.*, 2004], and from the MMCR using the algorithm of *Mace et al.* [2002]. For the MCRS retrieval, LWP is estimated from the ARM MW radiometer measurements as in *Lin et al.* [2001]. The LWP ranges from 4 (case number 9) to 85 g m^{-2} (case number 4) for these cases. As expected, the MCRS consistently produces smaller values of IWP than VISST. In all of the cases, the MCRS IWP is close to that from the MMCR retrieval. The differences are greatest for case 7 for which the LWP is 35 g m^{-2}, and the MCRS IWP is approximately 218 g m^{-2} less than the VISST retrieval. For these cases, the mean difference in IWP between the MCRS and MMCR is 9 g m^{-2}, which is 13.8% of the mean MMCR value of 65 g m^{-2} (Table 3). This bias is three times smaller than the parameterization-based MCRS result [*Huang et al.*, 2005] demonstrating the increase in accuracy that results from using explicit multi-layered cloud model calculations. The standard deviation of the differences is 30 g m^{-2}. The mean difference is almost 3.5 times smaller than the mean VISST-MMCR difference. *Huang et al.* [2006] found a similar difference (8%) when comparing satellite-based MCRS retrievals with MMCR retrievals taken from tropical Manus Island.

[32] It should be noted that radar retrievals of ice cloud properties have some inherent uncertainties, and comparisons of the properties from the tiny radar footprints against the much larger satellite pixel sizes introduce additional
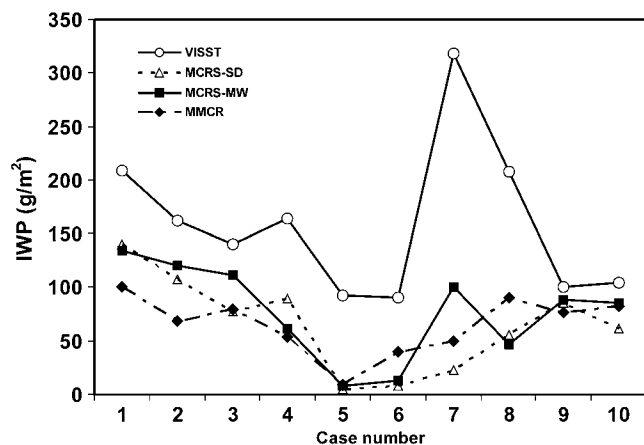

Figure 14. Comparison of IWP derived from MCRS with VISST and Millimeter Wave Cloud Radar (MMCR) reflectivity for 10 cases over ARM Southern Great Plains Central Facility.

Table 3. Means and Standard Deviations of IWP Derived From VISST, MCRS, and MMCR for Results in Figure 14

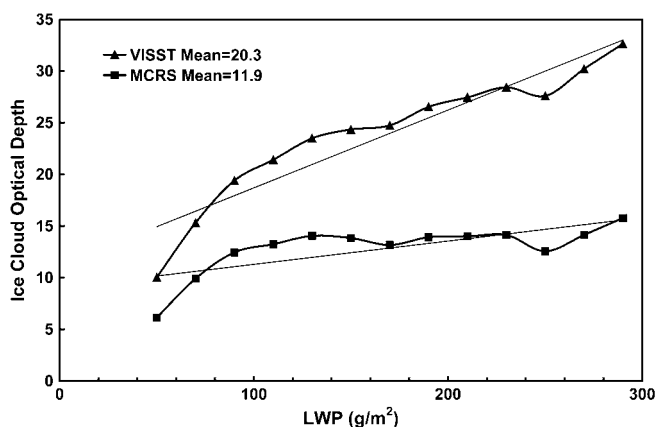|	VISST	MCRS	MCRS-SD	MMCR
Mean	158.8	74.3	59.7	65.1
Std. Dev.	71.5	43.56	44.03	27.3

Figure 15. Variation of optical depth derived from VISST and MCRS as a function of LWP_T for overcast ice-over-water cloud TMI pixels over ocean (30°S–30°N) during July 1998.

sources of error. The radar retrievals of ice particles are sensitive to the sixth moment of the size distribution, whereas the VISST optical depth retrieval is primarily dependent on the second moment. These different sensitivities can introduce some biases, especially when small ice crystals contribute significantly to the ice mass. Nevertheless, for clouds with IWP < 100 g m^{-2}, the Z-radiance radar technique used by *Mace et al.* [2005] yields values of IWP that have an RMS error of 25% compared to in situ measurements. The uncertainties in IWP derived with the Z-velocity technique used here [*Mace et al.*, 2002] are estimated to be on the order of ±50%. The errors associated with comparing measurements from narrow-beam sensors on the ground with relatively low-resolution satellite imager pixels have been discussed at length elsewhere (e.g., *Dong et al.* [2002], *Mace et al.* [2005], *Min et al.* [2005]) and are not reiterated here. The space-time differences tend to produce random, not bias errors. The differences between the MCRS and the MMCR retrievals are within the expected error of the Z-velocity method.

[33] Although the comparisons in Figure 14 and those presented by *Huang et al.* [2006] are quite limited, it is clear that the MCRS represents a marked improvement over the SL VISST retrieval. The MCRS reduces the TWP, on average, due to the lower value of IWP. Analyses of additional matched satellite data retrievals with fully validated ground observations are required to determine the overall accuracy of the MCRS. Nevertheless, the initial results indicate that the MCRS yields IWP values that are as accurate as SL VISST retrievals [e.g., *Mace et al.*, 2005] relative to the MMCR estimates.

[34] Figure 14 includes an additional set of data points labeled as MCRS-sounding data or MCRS-SD. These represent results based on the MCRS using GOES-8 data and LWP_{SD}, which is estimated from ARM SCF rawinsonde soundings using

$$LWP_{SD} = \int_{Z_B}^{Z_T} \eta(RH, T) * LWC(Z) dZ \qquad (3)$$

where Z_B and Z_T are the cloud base and top heights, respectively, and $\eta(RH, T)$ is the cloud probability function

that is determined from relative humidity RH and temperature T [*Minnis et al.*, 2005a, 2005b]. LWC is the adiabatic liquid water content. This algorithm, defined as the MCRS-SD, yields values of IWP that are as close to the MMCR results as the standard MCRS, which uses the MW radiometer retrievals of LWP. The mean MCRS-SD IWP (60 g m^{-2}) is smaller than both the MCRS and MMCR values. These results suggest that reliable soundings could be used as substitutes for MW radiometer data in the MCRS over land surfaces.

5.2. Dependencies

[35] Figure 15 shows a comparison of ice cloud optical depths derived from VISST and MCRS as a function of LWP for the July 1998 results. For the VISST retrievals, τ_I increases almost linearly with rising LWP. This is expected because thin water clouds will not cause a large VISST retrieval error, which is also consistent with the AD calculations (cf. Figures 2 and 3). The rise in R_v with increasing LWP causes the VISST to overestimate τ_I. The effects of the lower-layer cloud, however, are nearly removed by the MCRS; there is only a slight downward trend in the MCRS-retrieved τ_I associated with increasing LWP for LWP > 110 g m^{-2}. The mean τ_I drops to 7.7 from 13.9, a value very close to the mean for SL ice clouds (7.8) for the same number of samples within the domain. The variations of τ_I from VISST and MCRS as functions of T_w are shown in Figure 16. MCRS retrieves significantly lower values of τ_I than VISST for all T_w bins. The ice cloud optical depth decreases with increasing T_w for both the VISST and MCRS optical depths. This result suggests that the ice clouds are generally thicker in ice-over-cool-water clouds than in IOWW clouds.

[36] The dependence of τ_I on SZA for both MCRS and VISST is plotted in Figure 17. The values of τ_I are relatively flat for SZA < 65° but increase for larger SZAs. This variation may be due to a greater occurrence of anvil and deep convective clouds during early morning and late afternoon hours than for other times over Tropics. However, it may also be the result of model errors since three-dimensional effects, not included in the retrieval models, are more pronounced at the higher SZAs. Additional research is necessary to determine how much of the effect is algorithmic and how much is due to actual changes in cloud thickness near the terminator times.
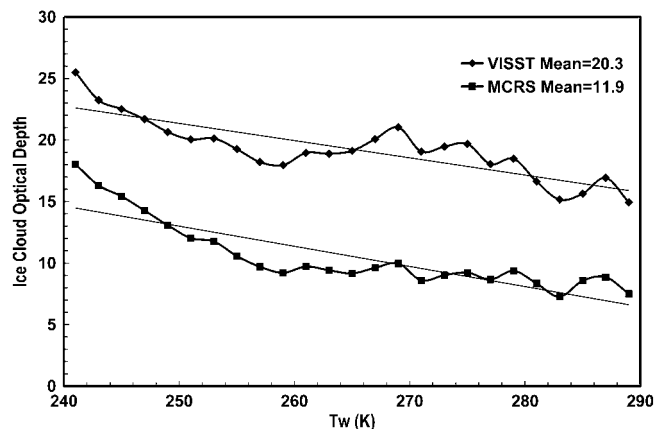

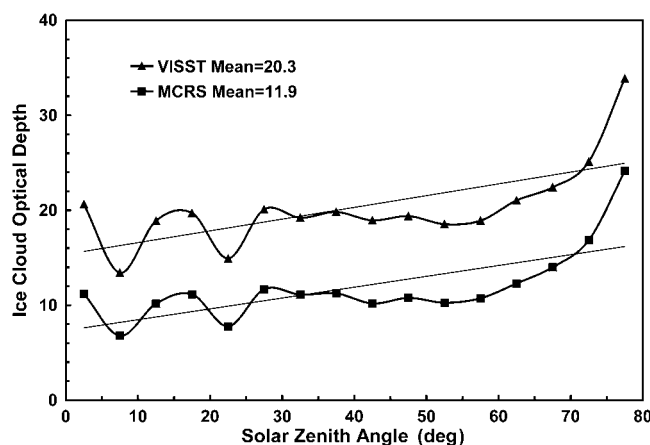**Figure 16.** Same as Figure 15, except as a function of Tw.

Figure 17. Same as Figure 15 except as function of solar zenith angle.

[37] Figure 18 compares the mean IWP derived from VISST, MVI, and MCRS as a function of LWP. The IWP derived from VISST represents the combined effects of all cloud layers; thus IWP = TWP. In that case, IWP increases substantially with increasing LWP just as τ_I did in Figure 15. The IWP derived from both MVI and MCRS have the same behavior, a small downward trend with increasing LWP for LWP > 110 g m^{-2}. In all cases, mean IWP from MVI is 10–50 g m^{-2} larger than that derived by the MCRS.

[38] Frequency distributions of τ_I are plotted in Figure 19 for the ICLD and MCRS OCLD cases. As noted earlier, the MVI picks up some OCLD cloud systems having $\tau_I < 0.25$, whereas the SL VISST retrieves no clouds with $\tau_I < 0.3$ and probably misses some clouds with $0.3 < \tau_I < 0.5$. The VIS signal is so weak in these instances that the CERES cloud detection algorithm misses many of those thin clouds. However, the enhanced VIS reflectance due to the lower-level cloud in the ML pixels ensures that the thinner ice clouds are included in the retrievals. Thus approximately 8% of the MCRS ice clouds have $\tau_I < 0.5$ compared with less than 2% for the ICLD cases. SL ice clouds occur more frequently than OCLDs when τ_I is between 0.75 and about 10. The reverse is true when $\tau_I > 10$. This difference in distribution suggests that ice clouds are more likely to be thicker when the entire column is moist or unstable.

[39] Histograms of IWP derived from VISST, MVI, and MCRS for ice-over-water clouds and the IWP derived from VISST for SL ice clouds are shown in Figure 20. As expected, the mean IWP values derived from the MCRS in July 1998 (Figure 20b) are considerably less than those derived from VISST. The mean IWP decreases from 283 to 173 g m^{-2}, a value only 10% larger than the SL ice cloud (ICLD) mean value of 157 g m^{-2}. The multilayered cloud pixels with IWP < 100 g m^{-2} comprise more than 50% of the data for MCRS retrievals compared with only 18% for VISST retrievals. For the lowest category (IWP < 100 g m^{-2}), the MCRS frequency is only 6% less than the ICLD frequency. The MVI and ICLD frequency distributions are also similar but differ more in all bins compared with MCRS and ICLD. The first bin includes negative values of IWP derived using the MVI indicating that the MVI-MCRS IWP difference of less than 20 g m^{-2}

would be much larger if negative IWP retrievals were not included. Similar results are also found in all other analyzed months as seen for January 1998 (Figure 20a). In this case, the mean IWP from MCRS is 5% less than the ICLD mean. The agreement in each bin is even closer than seen in Figure 19b. Overall, the consistency in the MCRS OCLD and the VISST ICLD frequency distributions for all bins further demonstrates the improvements provided by the MCRS.

5.3. Comparisons With Other Large-Scale Data

[40] The occurrence frequencies and geographical distributions of OCLD in this analysis are nearly the same as those reported by HO3 and are not shown here. For discussing comparisons with other analyses, the reader is referred to the distribution of OCLD occurrence from Figures 9 and 10 of HO3. *Heidinger and Pavolonis* [2005] found that their patterns of OL clouds were similar to those of HO3, but they found slightly more OL cloud cover. The patterns of OL high cloud cover in the work of *Chang and Li* [2005b] for analyses of 2001 *Terra* Moderate Resolution Imaging Spectroradiometer (MODIS) data are quite similar to those of HO3 for July, but different for January over the Pacific and North Atlantic Oceans. A strong El Niño, underway during January 1998 that ended before July 1998, may explain the differences in the patterns seen in January. While difficult to determine precisely from disparate figures, the OCLD FOC from HO3 in the Tropics appears to be slightly greater than that in the work of *Chang and Li* [2005b]. More OL cloudiness is expected when using higher-resolution data like MODIS because the OCLD definition requires 100% ice cloud cover in the 20-km TMI footprint. That definition excludes the edges of large clouds and scattered cirrus over lower clouds. The apparent discrepancies between the comparisons of HO3 with the results of *Heidinger and Pavolonis* [2005] and *Chang and Li* [2005b] may be due to algorithmic differences. The latter may be more constrained in terms of τ_I.

[41] HO3 applied the MVI technique to the 1998 CERES Edition-1 VIRS data and found that the IWP for the OCLD data was 6–10% less than that for the ICLD TMI pixels. The MCRS applied to the Edition-2 data for the same period
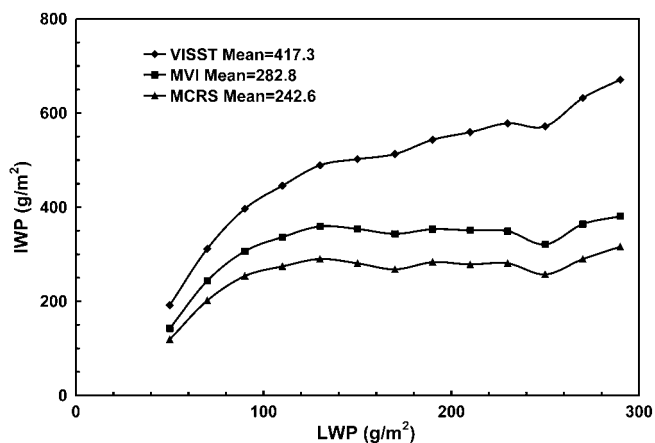

Figure 18. Mean IWP derived from VISST, MVI, and MCRS as a function of LWP$_T$ for overcast ice-over-water cloud TMI pixels over water surfaces (30°S–30°N) during July 1998.
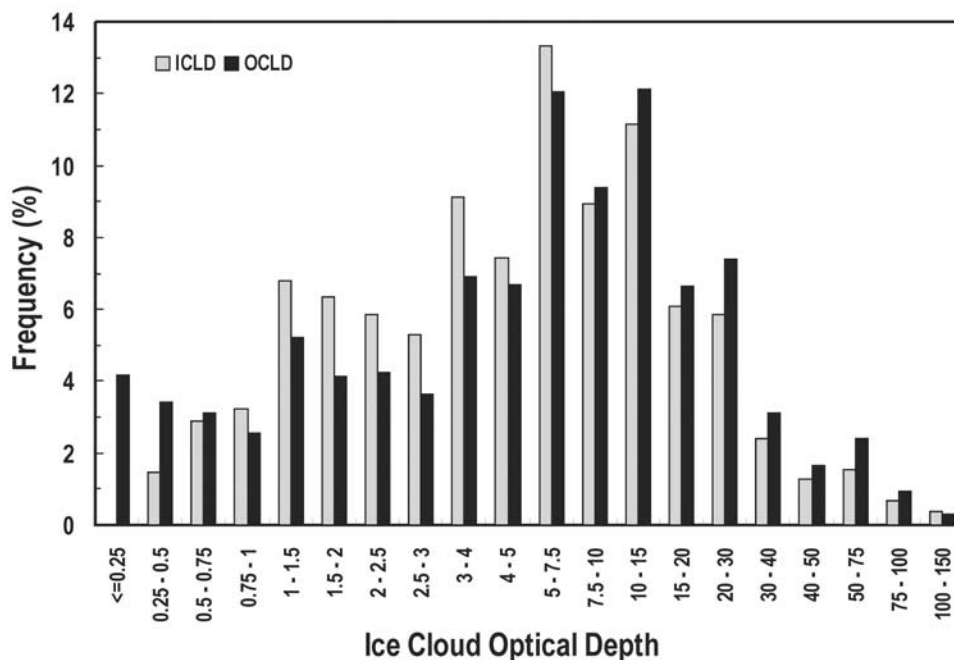
Figure 19. Frequency distribution of ice cloud optical depths derived using VISST for single-layered clouds (ICLD) from VIRS and using MCRS for overcast ice-over-water cloud from matched VIRS–TMI pixels over ocean between 30°S and 30°N during June, July, and August 1998.

yields OCLD IWP means that are 10% larger than the ICLD values, indicating some significant changes. *Chang and Li* [2005b] found that τ_I in the COVIR OL cloud cases ranged between 0 and 5 with an annual mean of 1.54 over ocean areas. This value is much smaller than the results in Table 2 and is clearly due to the limitations of applying the COVIR technique to optically thin high clouds. The MCRS detects and retrieves ice-over-water clouds regardless of τ_I, except when the clouds are precipitating. Nevertheless, the ratios of τ_I for OL clouds to that for SL clouds are similar for the two methods: 11% for the MCRS and 8% for *Chang and Li* [2005b] when the latter is based on the same classes of high clouds. A value of $\tau_I = 5$ corresponds to 94 g m^{-2} for De = 61 μm. Thus, the COVIR results correspond to roughly 53% of the MCRS OCLD results (i.e., IWP < 100 g m^{-2}) in Figure 19. The difference in FOC discussed earlier is most likely considerably less than 50%, so the OCLD cases do not account for all of the thin cirrus-over-water cloud cases. Thus, while there is commonality between OCLD and the results of *Chang and Li* [2005b], neither accounts for all OL clouds, even over ocean. Together, the two techniques should account for the impact of LWP in most ice-over-water clouds, but conditions where they provide overlapping results need to be defined. Neither technique can unscramble the relative contributions of LWP and IWP in precipitating clouds.

6. Concluding Remarks

[42] A more rigorous MCRS has been developed to improve the determination of high cloud properties in multilayered cloud systems over water surfaces. The MCRS attempts a more realistic interpretation of the radiance field than earlier methods because explicit radiative transfer calculations were used to simulate the observed radiances for two-layer cloud systems. Initial comparisons with independent data show that the MCRS produces a more accurate retrieval of IWP than the simple differencing techniques (e.g., MVI) used in the past. The MCRS method is quite appropriate for interpreting the radiances when the high cloud has a relatively large optical depth ($\tau_I > 2$). For thinner ice clouds, a more accurate retrieval might be possible using other methods. This issue needs further exploration.

[43] The results show that, compared to ice cloud properties derived using an SL cloud model, the MCRS reduces both the ice cloud optical depth and IWP by 42%, on average. Because the technique is more realistic and the preliminary validation data indicate good agreement with cloud radar retrievals, these new results should be considered more accurate than previous estimates of OL ice and water clouds in the Tropics. Hence they should be immediately valuable for assessing certain aspects of climate models. However, it is obvious that they only represent a portion of the OL cloud conditions.

[44] Despite the great strides made during the last few years in untangling the characteristics of OL cloud systems, many challenges remain in the effort to monitor the cloud water budget, especially for multilayered clouds. The current viable multilayer retrieval methods are applicable only during daytime and only in certain conditions. The COVIR approach can be used over most surfaces but is limited to optically thin clouds, whereas the MCRS is confined to ocean surfaces and cannot be used for precipitating clouds. Application of the MCRS over land would require either accurate knowledge of MW surface emissivities, which can be highly variable in time, or numerical weather analyses that provide reliable estimates of WV profiles in the lower troposphere. The latter could be used in the MCRS-
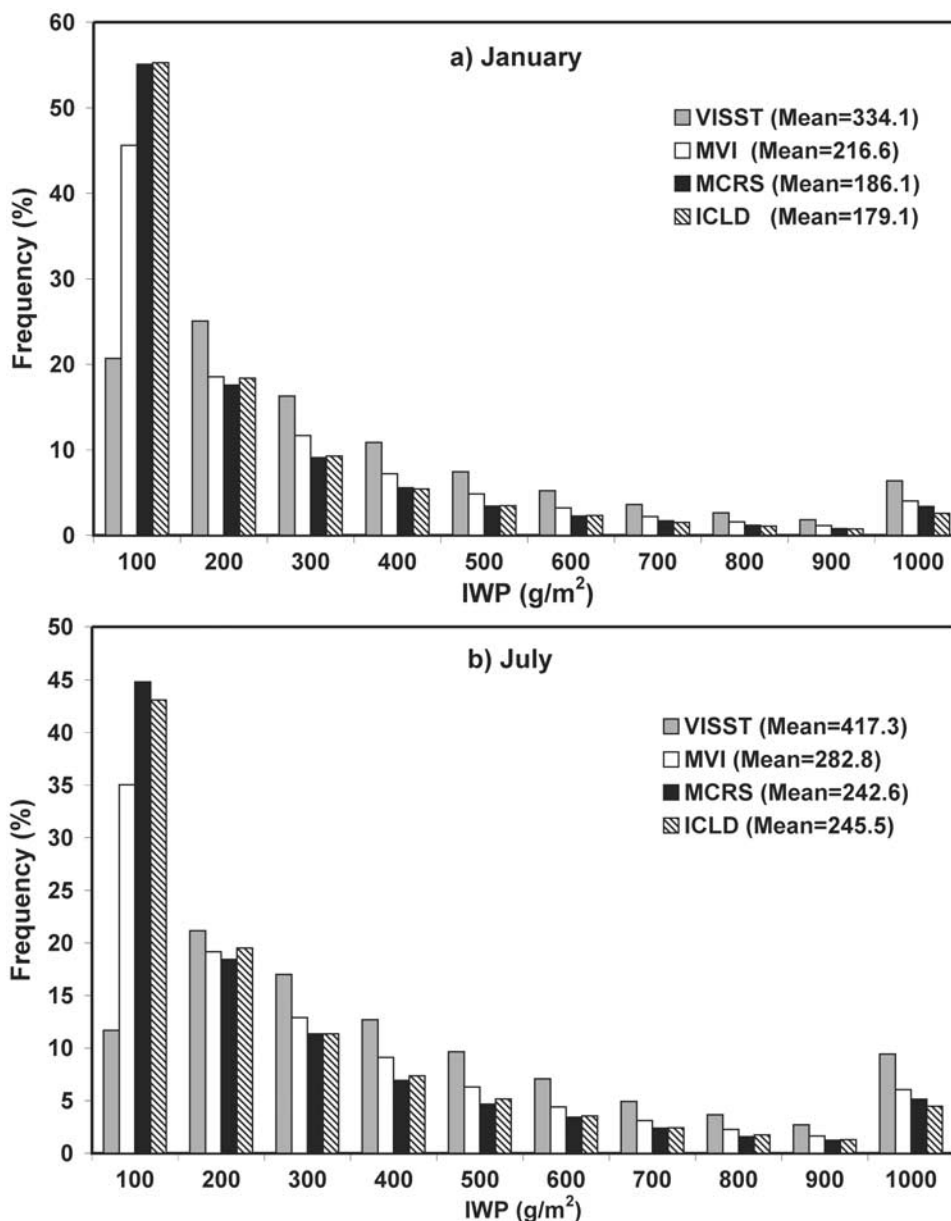
Figure 20. Histograms of IWP derived from VISST, MVI, and MCRS as functions of LWP$_T$ for overcast ice-over-water cloud TMI pixels over ocean between 30°S and 30°N during July 1998.

SD, as demonstrated in this study. For satellites lacking CO_2-slicing channels, the BTD method could be used to detect multilayered clouds, and a multispectral IR technique could be used to retrieve the upper-layer and lower-layer cloud properties as in the work of *Minnis et al.* [2005a, 2005b]. Assuming such techniques could be implemented, the problems of performing the retrievals at night and for precipitating clouds still remain. Perhaps, with the aid of the recently launched cloud radar on *CloudSat* [*Stephens et al.*, 2002] and the lidar on the Cloud Aerosol Lidar and Infrared Pathfinder Satellite Observations [CALIPSO; *Winker et al.*, 2002] satellites, current techniques can be further validated and improved, and new methods can be developed for retrieving multi-layered cloud properties at night from passive satellite imagery. As the current results demonstrate, however, the

MCRS can serve as an important component of any future comprehensive cloud monitoring system.

References

Arduini, R. F., P. Minnis, and D. F. Young (2002), Investigation of a visible reflectance parameterization for determining cloud properties in

multilayered clouds, *Proc. 11th AMS Conf. Cloud Physics*, Ogden, UT, June 3–7, CD-ROM, P2.4.

Chang, F.-L., and Z. Li (2005a), A new method for detection of cirrus overlapping water clouds and determination of their optical properties, *J. Atmos. Sci.*, *62*, 3993–4009.

Chang, F.-L., and Z. Li (2005b), A near-global climatology of single-layer and overlapped clouds and their optical properties from Terra/MODIS data using a new algorithm, *J. Clim.*, *18*, 4752–4771.

Dong, X., P. Minnis, G. G. Mace, W. L. Smith Jr., M. Poellot, R. T. Marchand, and A. D. Rapp (2002), Comparison of stratus cloud properties deduced from surface, GOES, and aircraft data during the March 2000 ARM Cloud IOP, *J. Atmos. Sci.*, *59*, 3256–3284.

Heidinger, A. K., and M. J. Pavolonis (2005), Global daytime distribution of overlapping cirrus cloud from NOAA's advanced very high resolution radiometer, *J. Clim.*, *18*, 4772–4784.

Ho, S.-P., B. Lin, P. Minnis, and T.-F. Fan (2003), Estimation of cloud vertical structure and water amount over tropical oceans using VIRS and TMI data, *J. Geophys. Res.*, *108*(D14), 4419, doi:10.1029/2002JD003298.

Huang, J., P. Minnis, B. Lin, Y. Yi, M. M. Khaiyer, R. F. Arduini, and G. G. Mace (2005), Advanced retrievals of multilayered cloud properties using multisensor and multispectral measurements, *J. Geophys. Res.*, *110*, D15S18, doi:10.1029/2004JD005101.

Huang, J., P. Minnis, B. Lin, Y. Yi, T.-F. Fan, S. Sun-Mack, and J. K. Ayers (2006), Determination of ice water path in ice-over-water cloud systems using combined MODIS and AMSR-E measurements, *Geophys. Res. Lett.*, *33*, L21801, doi:10.1029/2006GL027038.

Kummerow, C., W. Barnes, T. Kozu, J. Shiue, and J. Simpson (1998), The Tropical Rainfall Measuring Mission (TRMM) sensor package, *J. Atmos. Oceanic Technol.*, *15*, 809–817.

Lin, B., and W. B. Rossow (1996), Seasonal variation of liquid and ice water path in non-precipitating clouds over oceans, *J. Clim.*, *9*, 2890–2902.

Lin, B., B. Wielicki, P. Minnis, and W. B. Rossow (1998a), Estimation of water cloud properties from satellite microwave, infrared and visible measurements in oceanic environments, I: Microwave brightness temperature simulations, *J. Geophys. Res.*, *103*, 3873–3886.

Lin, B., P. Minnis, B. Wielicki, D. R. Doelling, R. Palikonda, D. F. Young, and T. Uttal (1998b), Estimation of water cloud properties from satellite microwave, infrared and visible measurements in oceanic environments, II: Results, *J. Geophys. Res.*, *103*, 3887–3905.

Lin, B., P. Minnis, A. Fan, J. A. Curry, and H. Gerber (2001), Comparison of cloud liquid water paths derived from in situ and microwave radiometer data taken during the SHEBA/FIREACE, *Geophys. Res. Lett.*, *28*, 975–978.

Mace, G. G., A. J. Heymsfield, and M. R. Poellot (2002), On retrieving the microphysical properties of cirrus clouds using the moments of the millimeter-wavelength Doppler spectrum, *J. Geophys. Res.*, *107*(D24), 4815, doi:10.1029/2001JD001308.

Mace, G. G., Y. Zhang, S. Platnick, M. D. King, P. Minnis, and P. Yang (2005), Evaluation of cirrus cloud properties from MODIS radiances using cloud properties derived from ground-based data collected at the ARM SGP site, *J. Appl. Meteorol.*, *44*, 221–240.

McClatchey, R. A., R. W. Fenn, J. E. A. Selby, F. E. Volz, and J. S. Garing (1973), Optical properties of the atmosphere (3rd edition), *AFCGRL-72-0497*, 113 pp. [NTIS-N73-18412].

Min, Q., P. Minnis, and M. M. Khaiyer (2004), Comparison of cirrus optical depths from GOES-8 and surface measurements, *J. Geophys. Res.*, *109*, D15207, doi:10.1029/2003JD004390.

Minnis, P., Y. Takano, and K.-N. Liou (1993), Inference of cirrus cloud properties using satellite-observed visible and infrared radiances, part I: Parameterization of radiance fields, *J. Atmos. Sci.*, *50*, 1279–1304.

Minnis, P., D. P. Kratz, J. A. Coakley Jr., M. D. King, D. P. Garber, P. W. Heck, S. Mayor, D. F. Young, and R. F. Arduini (1995), Cloud Optical Property Retrieval (Subsystem 4.3), Clouds and the Earth's Radiant Energy System (CERES) Algorithm Theoretical Basis Document, Volume III: Cloud Optical Property Retrieval (Subsystem 4.3), *NASA RP 1376 Vol. III*, edited by CERES Science Team, pp. 135–176.

Minnis, P., D. P. Garber, D. F. Young, R. F. Arduini, and Y. Takano (1998), Parameterization of reflectance and effective emittance for satellite remote sensing of cloud properties, *J. Atmos. Sci.*, *55*, 3313–3339.

Minnis, P., D. F. Young, B. A. Wielicki, P. W. Heck, X. Dong, L. L. Stowe, and R. Welch (1999), CERES cloud properties derived from multispectral VIRS data, *Proc. The EOS/SPIE Symposium on Remote Sensing, Vol. 3867*, Florence, Italy, September 20–24, 91–102.

Minnis, P., D. F. Young, B. A. Wielicki, D. P. Kratz, P. W. Heck, S. Sun-Mack, Q. Z. Trepte, Y. Chen, S. L. Gibson, R. R. Brown (2002), Seasonal and diurnal variations of cloud properties derived for CERES from VIRS and MODIS data, *Proc. 11th AMS Conf. Atmos. Rad.*, Ogden, UT, June 3–7, 20–23.

Minnis, P., L. Nguyen, W. L. Smith Jr., M. M. Khaiyer, R. Palikonda, D. A. Spangenberg, D. R. Doelling, D. Phan, G. D. Nowicki, P. W. Heck, and C. Wolff (2004), Real-time cloud, radiation, and aircraft icing parameters from GOES over the USA, *Proc. 13th AMS Conf. Satellite Oceanogr. and Meteorol.*, Norfolk, VA, Sept. 20–24, CD-ROM, P7.1.

Minnis, P., S. Sun-Mack, Y. Chen, H. Yi, J. Huang, L. Nguyen, and M. M. Khaiyer (2005a), Detection and retrieval of multi-layered cloud properties using satellite data, *Proc. SPIE Europe Intl. Symp. Remote Sens., Remote Sens. Clouds and Atmos. X, Bruges*, Belgium, September 19–22, *5979*, 597909, 9 pp.

Minnis, P., Y. Yi, J. Huang, and J. K. Ayers (2005b), Relationships between radiosonde and RUC-2 meteorological conditions and cloud occurrence determined from ARM data, *J. Geophys. Res.*, *110*, D23204, doi:10.1029/2005JD006005.

Pavolonis, M. J., and A. K. Heidinger (2004), Daytime cloud overlap detection using AVHRR and VIIRS, *J. Appl. Meteorol.*, *43*, 762–778.

Stephens, G. L., et al. (2002), The CloudSat mission and the A-Train, *Bull. Am. Meteorol. Soc.*, *83*, 1771–1790.

Wielicki, B. A., et al. (1998), Clouds and the Earth's Radiant Energy System (CERES): Algorithm overview, *IEEE Trans. Geosci. Remote Sens.*, *36*, 1127–1141.

Winker, D. M., J. Pelon and M. P. McCormick (2002), The CALIPSO mission: Spaceborne lidar for observation of aerosols and clouds, *SPIE Asia-Pacific Symposium on Remote Sensing of the Atmosphere, Environment and Space*, Hangzhou, China, 23–27 October, 4893-01.

————————————

R. F. Arduini, J. K. Ayers, T.-F. Fan, and Y. Yi, Science Systems and Applications, Inc., Hampton, VA 23666, USA.

J. Huang, College of Atmospheric Sciences, Lanzhou University, Lanzhou, China.

B. Lin and P. Minnis, NASA Langley Research Center, Hampton, VA 23681, USA.

G. G. Mace, Department of Meteorology, University of Utah, Salt Lake City, UT 84122, USA.